Journal of Scientific Computing, Vol. 20, No. 1, February 2004 (© 2003)

Technical Note

Spectral (Finite) Volume Method for Conservation Laws on Unstructured Grids III: One Dimensional Systems and Partition Optimization

Z. J. Wang[1] and Y. Liu[2]

Received April 21, 2002; accepted (in revised form) February 5, 2003

In this paper, the third in a series, the Spectral Volume (SV) method is extended to one-dimensional systems—the quasi-1D Euler equations. In addition, several new partitions are identified which optimize a certain form of the Lebesgue constant, and the performance of these partitions is assessed with the linear wave equation. A major focus of this paper is to verify that the SV method is capable of achieving high-order accuracy for hyperbolic systems of conservation laws. Both steady state and time accurate problems are used to demonstrate the overall capability of the SV method.

KEY WORDS: High-order; unstructured grid; spectral volume; system of conservation laws; Euler equations.

1. INTRODUCTION

We continue the development of the Spectral (Finite) Volume (SV) method for hyperbolic conservation laws on unstructured grids following the basic formulation [19] and development for two-dimensional scalar conservation laws [20]. The ultimate goal of this research is to pursue a numerical

[1] Associate Professor of Mechanical Engineering, Michigan State University, 2555 Engineering Building, East Lansing, Michigan 48824. E-mail: zjw@egr.msu.edu

[2] NASA Ames Research Center, Mail Stop T27B-1, Moffett Field, California 94035. E-mail: liu@nas.nasa.gov

0885-7474/04/0200-0137/0 © 2003 Plenum Publishing Corporation

method for conservation laws which has all of the following properties: (a) conservative, (b) high-order accuracy, i.e., the order of accuracy is greater than second order, (c) geometrically flexible, i.e., applicable for unstructured grids, and (d) computationally efficient. The SV method is developed to hopefully satisfy these four requirements, in a relative sense with respect to the current state-of-the-art numerical methods such as the high-order k-exact finite volume (FV) method [2, 3], essentially non-oscillatory (ENO) and weighted ENO (WENO) methods [1, 9, 12, 13], and the discontinuous Galerkin (DG) method [5–7], amongst many others.

Ultimately, the SV method is a Godunov-type finite volume method [10], which has been under development for several decades, and has become the-state-of-the-art for the numerical solution of hyperbolic conservation laws. For a more detailed review of the literature on the Godunov-type method, refer to [19], and the references therein. Similar to the Godunov method, the SV method has two key components. One is data reconstruction, and the other is the (approximate) Riemann solver. What distinguishes the SV method from the k-exact finite volume (FV) method is the data reconstruction. Instead of using a (large) stencil of neighboring cells to perform a high-order polynomial reconstruction, the unstructured grid cell—called a spectral volume—is partitioned into a "structured" set of sub-cells called control volumes (CVs), and cell-averages on these sub-cells are then the degrees-of-freedom (DOFs). These DOFs are used to perform a high-order polynomial reconstruction inside the SV. All the spectral volumes are partitioned in a geometrically similar manner, and thus a single reconstruction is obtained. Next, the DOFs are updated to high-order accuracy using the usual Godunov method. Numerical tests with scalar conservation laws in both 1D and 2D have verified that the SV method is indeed highly accurate, conservative, and geometrically flexible [20].

In this paper, we further extend the *SV* method to one-dimensional systems. In the next section, we present the SV method for the quasi-1D Euler equations. In Sec. 3, several convergent new partitions are developed by minimizing some approximate forms of the Lebesgue constant, and they are compared with the partition using the Gauss–Lobatto points. In Sec. 4, numerical tests with both steady state and time accurate unsteady problems are used to assess the performance of the SV method. In addition, the TVD and TVB limiters are tested with problems with discontinuities and complex smooth features. Furthermore, the performance of the various partitions is assessed in an accuracy study. Finally, conclusions and recommendations for further investigations are summarized in Sec. 5.

2. SPECTRAL VOLUME METHOD FOR THE QUASI-1D EULER EQUATIONS

The unsteady quasi-1D Euler equation in conservative form can be written as

$$\frac{\partial Q}{\partial t}+\frac{\partial F}{\partial x}=G, \tag{2.1a}$$

where Q is the vector of conserved variables, F is the inviscid flux vector, and G is the vector for the source terms given below:

$$Q=\begin{Bmatrix}\rho\\ \rho u\\ E\end{Bmatrix}, \qquad F=\begin{Bmatrix}\rho u\\ \rho u^2+p\\ u(E+p)\end{Bmatrix}, \qquad G=\begin{Bmatrix}-\rho u\dfrac{1}{A}\dfrac{\partial A}{\partial x}\\ -\rho u^2\dfrac{1}{A}\dfrac{\partial A}{\partial x}\\ -u(E+p)\dfrac{1}{A}\dfrac{\partial A}{\partial x}\end{Bmatrix}. \tag{2.1b}$$

Here ρ is the density, u is the velocity, p is the pressure, E is the total energy, and A is the area of the cross section. If $A=1$, the above equations degenerate into the 1D Euler equations. The pressure is related to the total energy by

$$E=\frac{p}{\gamma-1}+\frac{1}{2}\rho u^2, \tag{2.1c}$$

with $\gamma=1.4$ for air. Given a partition of the domain $[a, b]$, $\{x_{i+1/2}\}_{i=0}^{N}$, the domain is then divided into N non-overlapping spectral volumes (SVs)

$$[a, b]=\bigcup_{i=1}^{N} S_i, \qquad S_i=[x_{i-1/2}, x_{i+1/2}], \tag{2.2}$$

with $x_{1/2}=a$, and $x_{N+1/2}=b$. Let $h_i=x_{i+1/2}-x_{i-1/2}$, and denote the quantity $\max_{1\leqslant i\leqslant N} h_i$ by h. Given a desired order of accuracy k for (2.1), each spectral volume S_i is then partitioned into k control volumes (CVs) using the following partitioning $\{x_{i,j+1/2}\}_{j=0}^{k}$ with $x_{i,1/2}=x_{i-1/2}$ and $x_{i,k+1/2}=x_{i+1/2}$. The jth CV of S_i is then $C_{i,j}=(x_{i,j-1/2}, x_{i,j+1/2})$. The solution unknowns or degrees-of-freedom (DOFs) are the CV-averaged conserved

variables. These DOFs are then used to form high-order polynomials inside the SV. The integration of (2.1) in $C_{i,j}$ gives

$$\frac{dQ_{i,j}}{dt} h_{i,j} + (\hat{F}_{i,j+1/2} - \hat{F}_{i,j-1/2}) = \int_{x_{i,j-1/2}}^{x_{i,j+1/2}} G\, dx, \tag{2.3}$$

where $Q_{i,j}$ is the CV-averaged state vector, $h_{i,j} = x_{i,j-1/2} - x_{i,j+1/2}$, $\hat{F}_{i,j+1/2}$ is the Riemann flux computed using either the Roe [15] or Lax–Friedrichs solvers. The volume integral is carried out with a Gauss quadrature formula of appropriate order of accuracy. For time integration, we employ the third-order TVD Runge–Kutta scheme from [16].

3. OPTIMIZATION OF SPECTRAL VOLUME PARTITION

It has been found in [19, 20] that the stability and convergence of the SV method hinge on the partition of the SVs into CVs. It was shown that high-order ($>$ 3rd) accurate SV schemes are not grid convergent if the SV is partitioned into uniform CVs. This is believed similar to the so-called Runge phenomenon in Lagrange interpolation using equidistant grid points. An intuitive explanation given in [19] is that the basis functions using equidistant CVs are highly oscillatory near the two end points. As a result, instabilities are generated in the numerical solution, which become more pronounced when the grid is refined. To remedy this problem, the Gauss–Lobatto points were used to partition a SV [19], and the resultant "shape" functions were shown to be much less oscillatory than those employing uniform CVs. Numerical experiments did verify that uniform high-order accuracy was achieved with grid refinement. Although the partition using the Gauss–Lobatto points is grid-convergent, the question we raise here is whether we can do even better. It has never been shown that the Gauss–Lobatto points are the optimal choice in any sense.

For this purpose, we consider the standard interval $D = [-1, 1]$ as the SV since each SV can be linearly transformed into D. This interval is then divided into k CVs with the following $k+1$ grid points:

$$-1 = x_{i,1/2} < x_{i,3/2} < \cdots < x_{i,k+1/2} = 1,$$

which is called a partition denoted by Π of D. For each $u(x) \in \mathscr{C}(D)$ (the space of all continuous functions), we can reconstruct a polynomial $p_i(x) \in P^{k-1}(D)$ from the CV-averaged solution $\bar{u}_{i,j}$, which satisfies

$$p_i(x) = \sum_{j=1}^{k} L_j(x)\, \bar{u}_{i,j}. \tag{3.1}$$

Denote $p_i = \Gamma_\Pi(u)$, where Γ_Π is an operator which maps $\mathscr{C}(D)$ onto $P^{k-1}(D)$. It is obvious that Γ_Π is a linear projection operator. When both spaces $\mathscr{C}(D)$ and $P^{k-1}(D)$ are equipped with the supremum or uniform norm, i.e., $\|\bullet\| = \|\bullet\|_\infty = \max|\bullet|$, the norm of this projection operator can be defined as

$$\|\Gamma_\Pi\| = \sup_{u \neq 0} \frac{\|\Gamma_\Pi u\|}{\|u\|}. \tag{3.2}$$

Therefore we can easily see that

$$\|\Gamma_\Pi\| = \max_{x \in D} \sum_{j=1}^{k} |L_j(x)|. \tag{3.3}$$

The function $\lambda(x) = \sum_{j=1}^{k} |L_j(x)|$ is usually referred to as the Lebesgue function of the interpolation, and $\|\Gamma_\Pi\|$ is called the Lebesgue constant [4], which is of interest because

- If p_i^* is the best uniform approximation to u on E, then

$$\|u - \Gamma_\Pi u\| \leqslant (1 + \|\Gamma_\Pi\|)\, \|u - p_i^*\|. \tag{3.4}$$

Thus $\|\Gamma_\Pi\|$ gives a simple method of bounding the interpolation polynomial. It is obvious from (3.4) that the smaller the Lebesgue constant, the better the interpolation polynomial is to be expected in the uniform norm. Therefore the partition optimization problem becomes finding the partition with the smallest Lebesgue constant. Because the Lebesgue function is a non-differential function, it is very difficult to find the optimum partition. However, given any partition, the Lebesgue constant can be computed numerically. In [19], it has been shown that the Gauss–Lobatto points defined by

$$x_{i,\, j+1/2} = -\cos\left(\frac{j\pi}{k}\right), \qquad j = 0, \ldots, k, \tag{3.5}$$

result in convergent SV schemes. The Lebesgue constants for both equidistant and the Gauss–Lobatto points are given in Table I. Note that the Lebesgue constants for the uniform CVs increase super-linearly with respect to k, while the Lebesgue constant for the Gauss–Lobatto points increase slowly with increasing k. In fact, the Lebesgue constant for $k = 4$ with uniform CVs is larger than that for $k = 8$ with Gauss–Lobatto points. The partition using the Gauss–Lobatto points is denoted by Π_{GL}, and the optimum partition with the minimum Lebesgue constant is denoted by Π_∞.

Table I. Lebesgue Constants for Several Partitions

k	Uniform Grid	Π_{GL}	Π_2	$\Pi_{\mu,\infty}$
2	2.000	2.000	2.000	2.000
3	3.333	2.667	2.215	1.685
4	5.333	3.172	2.475	1.823
5	8.533	3.578	2.662	2.141
6	13.87	3.917	2.817	2.534
7	23.01	4.208	2.945	2.790
8	39.01	4.463	3.055	3.192

Because of the difficulty in computing Π_∞, we instead attempt to find the following partition (called Π_2) by minimizing [4]

$$\|\Gamma_\Pi\|_2 = \sqrt{\sum_{j=1}^{k} \int_{-1}^{1} L_j^2(x)\, dx}\,. \tag{3.6}$$

Obviously, the partitions Π_∞ and Π_2 are not expected to be the same, but they should not differ dramatically. Since $\|\Gamma_\Pi\|_2$ is differentiable with respect to the partitioning nodes, many standard minimization algorithms can be used to compute Π_2. The numerically computed Π_2 with $k = 3-8$ are presented in Table II.

Table II. Node Sets Which Minimize $\|\Gamma_\Pi\|_2 = \sqrt{\sum_{j=1}^{k} \int_{-1}^{1} L_j^2(x)\, dx}$

k	x_i
3	0.62392259
4	0.79174292
5	0.86971298 0.32686243
6	0.91060472 0.52380525
7	0.93493530 0.64667784 0.23314423
8	0.95052305 0.72820167 0.39718507

In [19], it was suggested that the following one-parameter family of nodes be used to partition the standard interval

$$x_{i,\,j+1/2} = \frac{\tanh\left(\dfrac{2\mu j}{k} - \mu\right)}{\tanh(\mu)}, \qquad j = 0,\ldots, k, \tag{3.7}$$

where μ is a constant, which controls the degree of grid clustering near the two end grid points. The larger the value of μ is, the stronger the grid clustering near -1 and 1. Numerical means can be easily used to find the approximate parameter μ, which gives the minimum Lebesgue constant in this family. The results are tabulated in Table III for $k = 3-8$. This partition is called $\Pi_{\mu,\infty}$. Test cases will be presented using the three different partitions (Π_{GL}, Π_2, $\Pi_{\mu,\infty}$) to see how they perform in a SV scheme. Just to give the readers a visual impression, the equidistant partition, Π_{GL}, Π_2, $\Pi_{\mu,\infty}$ and their corresponding basis functions are plotted in Fig. 1. In addition, the Lebesgue constants for the partitions are compared in Table I. Obviously the equidistant partition has the most oscillatory basis functions. Note that Π_{GL} is the most "uniform" (except the equidistant partition), followed by Π_2 and $\Pi_{\mu,\infty}$. Among the three partitions (Π_{GL}, Π_2, $\Pi_{\mu,\infty}$), Π_{GL} has the largest Lebesgue constants, and $\Pi_{\mu,\infty}$ has the smallest Lebesgue constant except $k = 8$, for which the Π_2 partition has the smallest Lebesgue constant.

Table III. Node Sets $\Pi_{\mu,\infty}$

k	x_i
3	0.78077641
4	0.87915287
5	0.90385565 0.44634975
6	0.91726962 0.63249867
7	0.93284494 0.73841123 0.30039009
8	0.94056849 0.79369782 0.48327169

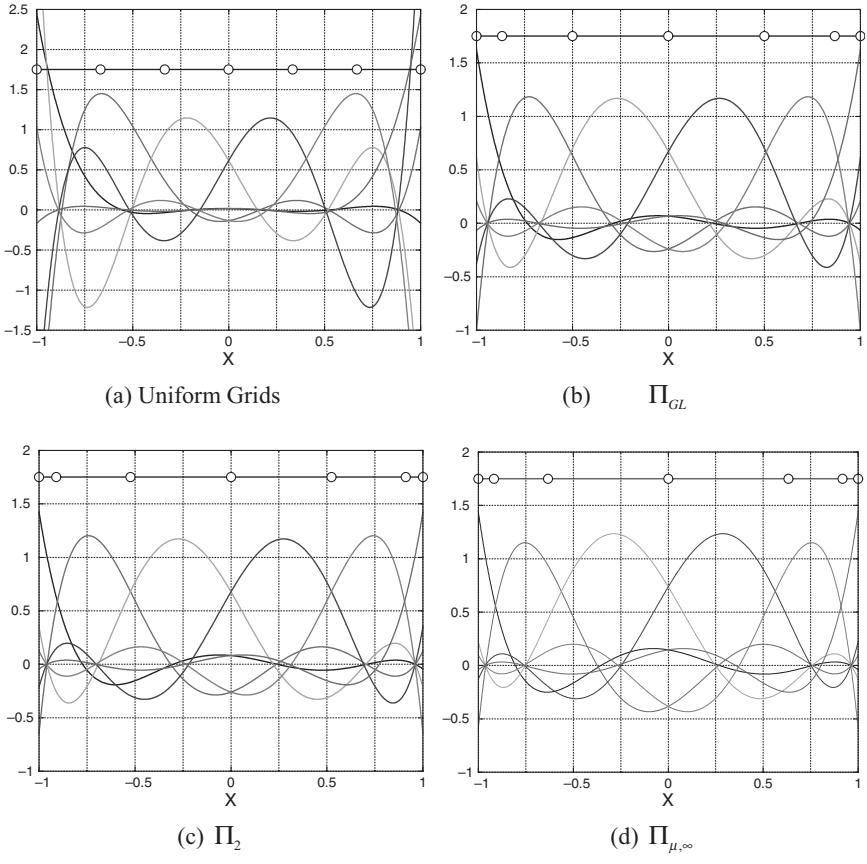

(a) Uniform Grids (b) Π_{GL}

(c) Π_2 (d) $\Pi_{\mu,\infty}$

Fig. 1. The basis functions and grid points of the three different partitions with $k = 6$.

4. NUMERICAL TESTS

4.1. Partition Evaluation

In this test, the performance of the three different partitions (Π_{GL}, Π_2, $\Pi_{\mu,\infty}$) is evaluated with the following scalar conservation law

$$\frac{\partial u}{\partial t}+\frac{\partial u}{\partial x}=0, \qquad -1 \leqslant x \leqslant 1$$

$$u(x, 0)=\sin(\pi x), \qquad \text{periodic boundary condition.}$$

The L_1 and L_∞ errors using the third-order and sixth-order SV schemes with the three partitions are presented in Table IV. For the third-order SV scheme, Π_{GL} yielded the least L_∞ error, followed by Π_2, while $\Pi_{\mu,\infty}$ produced the largest L_∞ error, although $\Pi_{\mu,\infty}$ has the minimum Lebesgue constant. The minimum L_1 error was produced by Π_2, followed by Π_{GL} and $\Pi_{\mu,\infty}$. For the third-order scheme, the partition with the minimum Lebesgue constant produced the largest errors. This may indicate that the Lebesgue constant cannot accurately predict the performance of the partition. For the sixth-order SV scheme, the Lebesgue constant turns out to be a more accurate indicator. $\Pi_{\mu,\infty}$ yielded the least L_∞ and L_1 errors, followed by Π_2, while Π_{GL} produced the largest L_∞ and L_1 errors, exactly following the prediction by the Lebesgue constant. Note that all three

Table IV. Accuracy Study of SV Schemes with Three Different Partitions

Partition	Order of Accuracy	NDOF	L_∞ error	L_∞ order	L_1 error	L_1 order
Π_{GL}	3	30	2.67e−3	–	1.24e−3	–
		60	3.65e−4	2.87	1.61e−4	2.95
		120	4.67e−5	2.97	2.05e−5	2.97
		240	5.91e−6	2.98	2.59e−6	2.98
	6	30	1.28e−5	–	2.57e−6	–
		60	1.88e−7	6.09	4.08e−8	5.98
		120	2.98e−9	5.98	6.47e−10	5.97
		240	4.61e−11	6.05	9.114e−12	5.96
Π_2	3	30	2.56e−3	–	1.19e−3	–
		60	3.57e−4	2.84	1.47e−4	3.02
		120	4.71e−5	2.92	1.84e−5	3.00
		240	6.04e−6	2.96	2.31e−6	2.99
	6	30	8.10e−6	–	2.19e−6	–
		60	1.57e−7	5.69	3.70e−8	5.89
		120	2.42e−9	6.02	5.71e−10	6.02
		240	3.81e−11	6.01	8.99e−12	6.04
$\Pi_{\mu,\infty}$	3	30	4.83e−3	–	2.99e−3	–
		60	6.52e−4	2.89	3.83e−4	2.96
		120	8.45e−5	2.95	4.86e−5	2.98
		240	1.07e−5	2.98	6.11e−6	3.99
	6	30	6.16e−6	–	2.89e−6	–
		60	1.01e−7	5.93	3.56e−8	6.34
		120	1.67e−9	5.92	5.77e−10	5.95
		240	2.54e−11	6.04	8.33e−12	6.11

partitions achieved the expected order of accuracy, and the differences between the results computed with the different partitions are quite small. From here on, we will use partition Π_{GL}.

4.2. Accuracy Study with a Steady 1D Flow through a Nozzle

In this accuracy study, we compute the numerical order of accuracy of the SV method using a steady subsonic quasi-1D flow through a converging nozzle with the following area variation

$$A(x) = 1.5 - 0.5 \tanh(x) \qquad -5 \leqslant x \leqslant 5.$$

The flow condition is so defined that an exit Mach number of 0.8 is produced. An analytical solution can be computed based on the isentropic flow assumption. The inflow and outflow conditions of the analytical solution are given below:

$$\{\rho_{in}, u_{in}, p_{in}\} = \{1.2949245, 0.30891936, 1.0256854\}$$
$$\{\rho_{out}, u_{out}, p_{out}\} = \{1, 0.8, 0.71428571\}.$$

In the accuracy study, uniform SV grids were used first. To compute the errors in the numerical solution, the CV-averaged densities are used to reconstruct the densities at the SV boundaries, which are then compared with the analytical solutions to determine the L_1 and L_∞ error norms. The SVs were partitioned with the Gauss–Lobatto points. In the first test, Roe's flux splitting was used to compute the numerical flux. The computed L_1 and L_∞ errors with SV schemes of various orders of accuracy on different grids are given in Table V. Note that the expected orders of accuracy for all the SV schemes are achieved in both the L_1 and L_∞ norms in this case.

Next, the performance of the local Lax–Friedrichs flux is tested, and the L_1 and L_∞ errors are summarized in Table VI. Again it is obvious that the expected orders of accuracy for all the SV schemes are achieved in both the L_1 and L_∞ norms. It can be observed that Roe's approximate Riemann solver produced more accurate numerical results on coarse grids for all the schemes tested. For the lower order schemes (2nd and 3rd order), Roe flux is consistently more accurate than the local Lax–Friedrichs flux on all the grids. However, it is interesting to note that the local Lax–Friedrichs flux produced slightly more accurate results using the 4th and 6th order schemes on the two finest meshes although the difference is quite small.

Table V. Accuracy of SV Schemes for Steady 1D Flow Through a Converging Nozzle Roe Splitting, Gauss–Lobatto Points, Uniform SVs

Order of Accuracy	NDOF	L_∞ error	L_∞ order	L_1 error	L_1 order
	24	1.40e−2	–	2.78e−3	–
	48	3.24e−3	2.11	5.42e−4	2.36
2	96	7.18e−4	2.17	1.15e−4	2.24
	192	1.57e−4	2.19	2.63e−5	2.13
	384	3.72e−5	2.08	6.25e−6	2.07
	24	8.69e−3	–	7.21e−4	–
	48	1.10e−3	2.98	9.77e−5	2.88
3	96	1.79e−4	2.62	1.39e−5	2.81
	192	2.64e−5	2.76	1.85e−6	2.91
	384	3.48e−6	2.92	2.36e−7	2.97
	24	5.66e−3	–	5.13e−4	–
	48	3.47e−4	4.03	2.56e−5	4.32
4	96	3.94e−5	3.14	1.55e−6	4.05
	192	1.88e−6	4.39	7.78e−8	4.32
	384	1.02e−7	4.20	4.09e−9	4.25
	24	1.75e−3	–	1.35e−4	–
	48	8.30e−5	4.39	3.66e−6	5.20
6	96	1.73e−6	5.58	5.77e−8	5.99
	192	4.80e−8	5.17	8.67e−10	6.06
	384	5.86e−10	6.36	1.10e−11	6.30

Finally the performance of the SV method with non-uniform SVs is assessed. The SVs were generated by perturbing the uniform grid 10% at each grid point. Therefore, the size of the largest SV is 50% bigger than the size of the smallest one. Roe's flux splitting and Π_{GL} were employed in the simulation, and the results are presented in Table VII. Note again that the designed orders of accuracy have been achieved by all the schemes in both the L_1 and L_∞ norms. It is obvious that the magnitudes of the errors are higher on the non-uniform grids than those on the uniform grids.

4.3. Blast Wave Interaction Problem

This problem was suggested by Colella and Woodward [8], and has been widely used to assess high-order accurate shock-capturing methods. It

Table VI. Accuracy of SV Schemes for Steady 1D Flow Through a Converging Nozzle Local Lax–Friedrichs Flux, Gauss–Lobatto Points, Uniform SVs

Order of Accuracy	NDOF	L_∞ error	L_∞ order	L_1 error	L_1 order
	24	1.89e−2	–	3.33e−3	–
	48	3.26e−3	2.54	4.93e−4	2.76
2	96	6.65e−4	2.29	1.07e−4	2.20
	192	1.51e−4	2.14	2.50e−5	2.10
	384	3.65e−5	2.05	6.08e−6	2.04
	24	1.19e−2	–	1.60e−3	–
	48	2.06e−3	2.53	1.73e−4	3.21
3	96	3.83e−4	2.43	4.09e−5	2.08
	192	5.76e−5	2.73	5.48e−6	2.90
	384	8.00e−6	2.85	7.20e−7	2.93
	24	1.61e−2	–	4.19e−3	–
	48	6.00e−4	4.74	1.12e−4	5.23
4	96	3.97e−5	3.92	1.60e−6	6.13
	192	1.81e−6	4.46	7.08e−8	4.50
	384	9.32e−8	4.28	3.84e−9	4.20
	24	3.63e−3	–	7.41e−4	–
	48	1.64e−4	4.47	4.33e−5	4.10
6	96	3.59e−6	5.51	4.78e−7	6.50
	192	5.30e−8	6.08	8.09e−10	9.20
	384	5.31e−10	6.64	9.72e−12	6.38

is selected here to test the shock capturing capability of the SV method. The initial conditions are

$$Q(x,0)=\begin{cases} Q_L, & 0\leqslant x\leqslant 0.1,\\ Q_M, & 0.1\leqslant x\leqslant 0.9\\ Q_R, & 0.9\leqslant x\leqslant 1, \end{cases}$$

where

$$\{\rho_L, u_L, p_L\}=\{1,0,1000\}$$
$$\{\rho_M, u_M, p_M\}=\{1,0,0.01\}$$
$$\{\rho_R, u_R, p_R\}=\{1,0,100\}.$$

The boundaries at $x=0$ and $x=1$ are solid walls. The simulation was carried out until $t=0.038$. For comparison purposes, a converged solution using a second-order MUSCL scheme on a grid of 3,200 cells is used as the

Table VII. Accuracy of SV Schemes for Steady 1D Flow Through a Converging Nozzle Roe Splitting, Gauss–Lobatto Points, Non-Uniform SVs

Order of Accuracy	NDOF	L_∞ error	L_∞ order	L_1 error	L_1 order
	24	2.16e−2	–	3.68e−3	–
	48	4.71e−3	2.20	5.93e−4	2.63
2	96	1.06e−3	2.15	1.30e−4	2.19
	192	2.66e−4	1.99	2.92e−5	2.15
	384	6.52e−5	2.03	6.93e−6	2.08
	24	5.68e−3	–	7.07e−4	–
	48	1.05e−3	2.44	8.48e−5	3.06
3	96	2.89e−4	1.86	1.64e−5	2.37
	192	3.60e−5	3.01	2.17e−6	2.92
	384	4.75e−6	2.92	2.76e−7	2.97
	24	9.84e−3	–	8.49e−4	–
	48	6.46e−4	3.93	4.03e−5	4.40
4	96	4.66e−5	3.79	2.36e−6	4.09
	192	2.88e−6	4.02	1.24e−7	4.25
	384	1.89e−7	3.93	7.06e−9	4.17
	24	2.14e−3	–	1.98e−4	–
	48	5.33e−5	5.32	4.09e−6	5.60
6	96	4.13e−6	3.69	9.68e−8	5.40
	192	6.61e−8	5.97	1.53e−9	5.98
	384	1.18e−9	5.81	2.51e−11	5.93

"exact" solution. Component-wise TVD limiters and Roe flux splitting were used in the computations. Gauss–Lobatto points were used to partition the SVs. The computed density profiles on two grids with 200 and 400 SVs using SV schemes of second to fourth orders are presented in Figs. 2 and 3. Obviously, the second-order scheme with 200 SVs was not able to capture the peak density, while the third and fourth order schemes did a far better job. Even with 400 SVs, the second-order scheme still failed to capture the density maximum, but the third and fourth-order schemes produced excellent results. Note that again the results computed with the SV method compare favorably to the results computed with the DG method presented in [6].

4.4. Shock-Acoustic Wave Interaction Problem

This case was suggested by Shu and Osher [18] to demonstrate the advantages of high-order schemes in capturing both discontinuities and

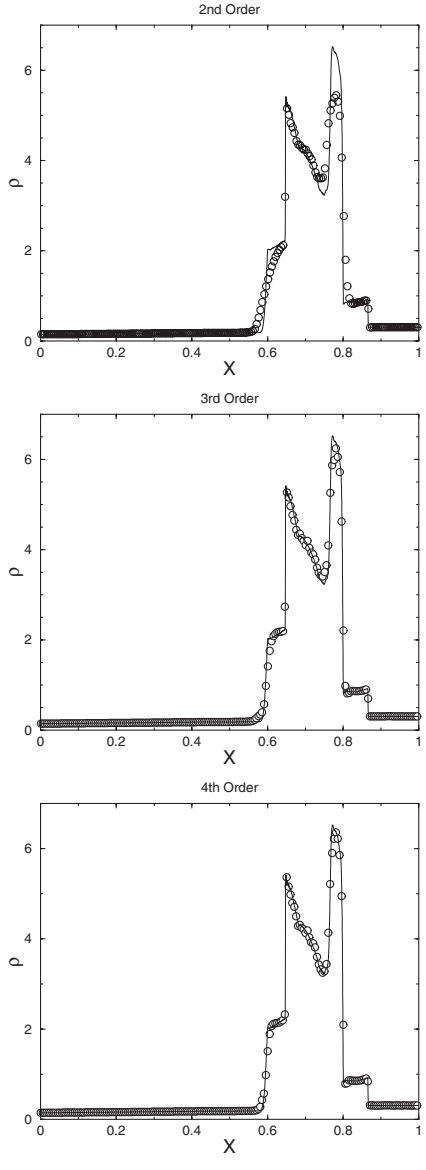

Fig. 2. Density profiles computed with second to fourth order SV schemes on 200 SVs with TVD Limiters. One data point from a SV is shown.

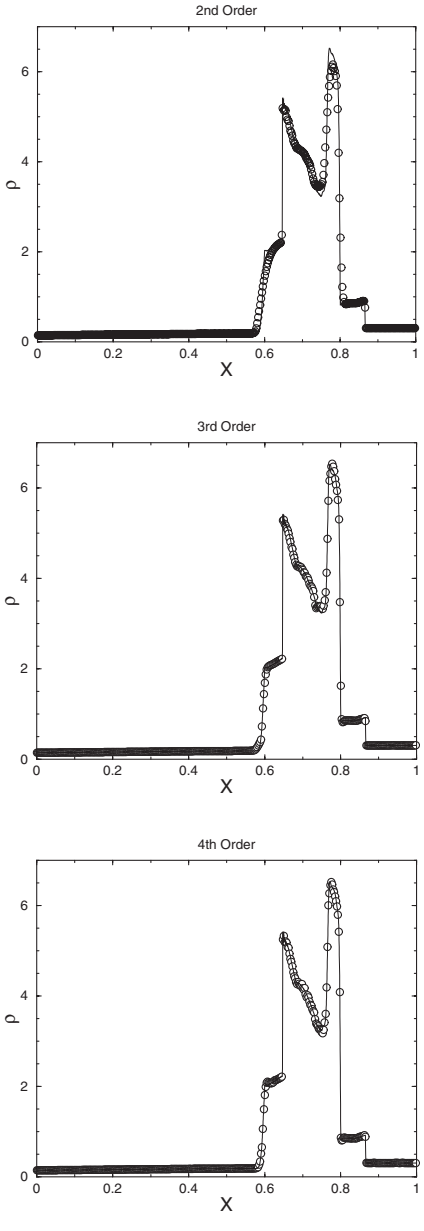

Fig. 3. Density profiles computed with second to fourth order SV schemes on 400 SVs with TVD limiters. One data point from a SV is shown.

complex smooth structures, such as those occurring in shock-acoustic wave interactions. The initial conditions are

$$Q(x, 0) = \begin{cases} Q_L, & x \leqslant -4, \\ Q_R, & x \geqslant -4, \end{cases}$$

where

$$\{\rho_L, u_L, p_L\} = \{3.857143, 2.629369, 10.333333\}$$
$$\{\rho_R, u_R, p_R\} = \{1 + 0.2 \sin(5x), 0, 1\}.$$

A converged solution using a second-order MUSCL scheme on a grid of 3,200 cells is used as the "exact" solution. Roe's flux splitting and Π_{GL} were employed in the simulation. Two uniform grids with 200 and 400 SVs were adopted. In the first set of tests, a TVD limiter was used, and the results are plotted in Figs. 4–5. On the coarse mesh, the second-order SV scheme heavily smeared the complex smooth structure, while the fourth-order SV scheme gave excellent results. The solution computed with the third-order SV scheme is between the results of second and fourth-order SV schemes. On the fine mesh, both the third and fourth-order schemes yielded excellent results, while the second-order scheme still smeared some of the density waves. We also tested the SV schemes with the same DOFs, and a TVB limiter using $M = 250$, and the results are shown in Fig. 6. Note that the smooth structures are much better resolved with the TVB limiter than with a TVD limiter. The results computed with the third and fourth-order SV schemes are excellent. A close-up view of the density profiles near the complex structure with both TVD and TVB limiters are shown in Fig. 7. Even with heavy limiting of the TVD limiter, the fourth-order scheme produced the best solution, and the second-order scheme gave the worst result. With a TVB limiter using a properly chosen M, both the third-order and fourth schemes produced excellent results, though the second-order scheme is still too dissipative.

5. CONCLUSIONS

The Spectral Volume method has been successfully extended to one-dimensional hyperbolic systems of conservation laws. In addition, several different partitions have been identified, and tested with the scalar conservation law. Although the Lebesgue constant is a good measure of partition quality, it cannot be used to definitely predict which partition gives better numerical solutions for a particular problem. All three partitions (Π_{GL}, Π_2, $\Pi_{\mu,\infty}$) achieved the expected order of accuracy, and are shown to be convergent.

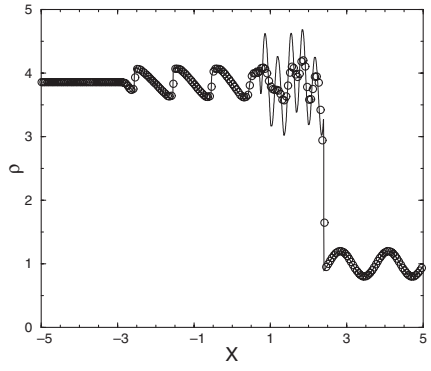

(a) 2nd Order

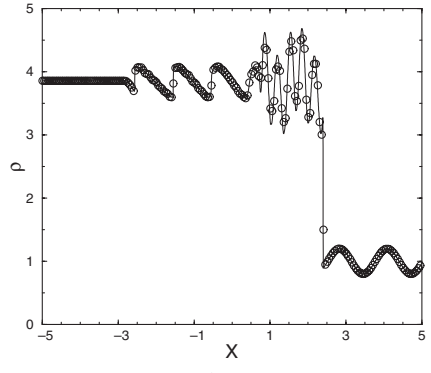

(b) 3rd Order

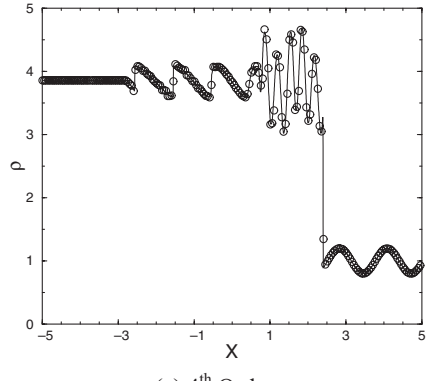

(c) 4th Order

Fig. 4. Density profiles computed with second to fourth order SV schemes on 200 SVs with TVD Limiters. One data point from a SV is shown.

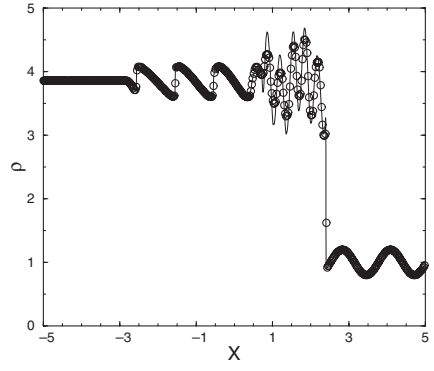

(a) 2nd Order

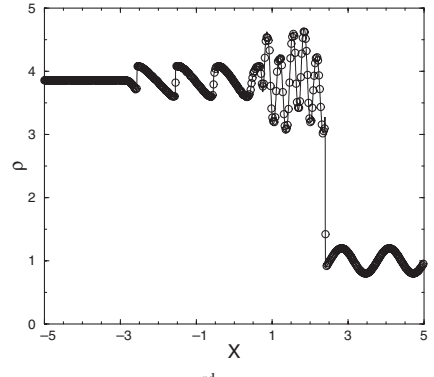

(b) 3rd Order

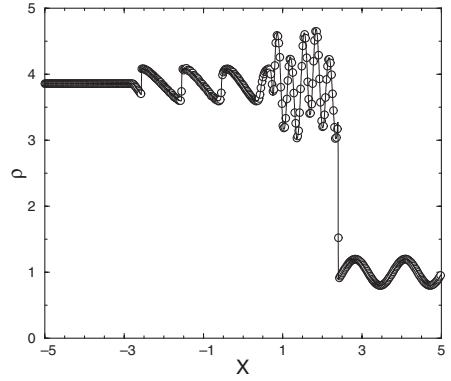

(c) 4th Order

Fig. 5. Density profiles computed with second to fourth order SV schemes on 400 SVs with TVD Limiters. One data point from a SV is shown.

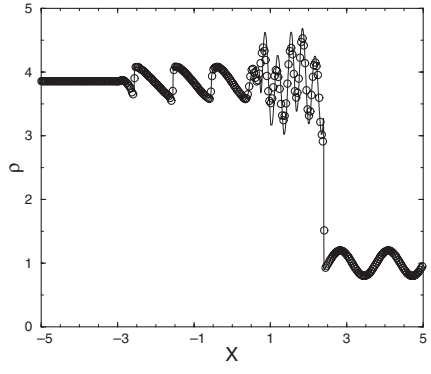

(a) 2nd Order

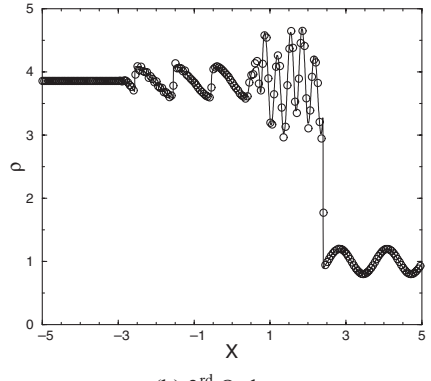

(b) 3rd Order

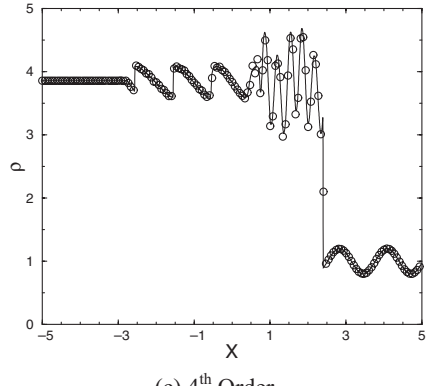

(c) 4th Order

Fig. 6. Density profiles computed with second to fourth order SV schemes using 600 DOFs and a TVB limiters (M = 250).

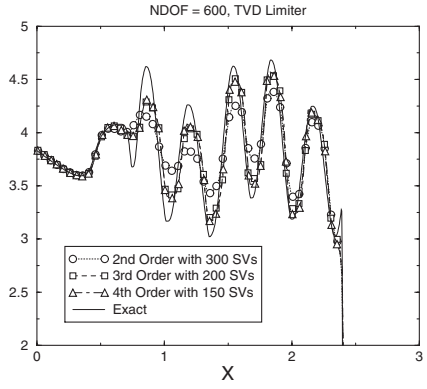

(a) TVD Limiter

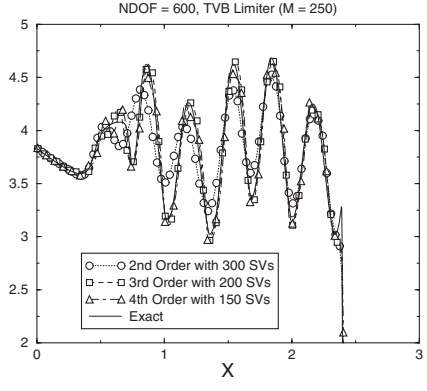

(b) TVB Limiter with M = 250

Fig. 7. Close-up view of the density profiles computed with second to fourth order SV schemes using 600 DOFs and TVD and TVB Limiters.

An accuracy study with a steady subsonic flow through a converging nozzle has verified that the designed high-order accuracy can be achieved in the system setting. The SV method performed very well for the unsteady cases with discontinuities, and both discontinuities and complex smooth structures. In particular, TVB limiters performed better than TVD limiters for smooth structures. The extension to 2D Euler equations is now under way, and will be reported in a future publication.

ACKNOWLEDGMENT

The first author grateful acknowledges an Intramural Research Grants Program from Michigan State University, and the start-up funding provided

by the Department of Mechanical Engineering, College of Engineering of Michigan State University.

REFERENCES

1. Abgrall, R. (1994). On essentially non-oscillatory schemes on unstructured meshes: analysis and implementation. *J. Comp. Phys.* **114**, 45–58.
2. Barth, T. J., and Jespersen, D. C. The design and application of upwind schemes on unstructured meshes, *AIAA*, Paper No. 89-0366.
3. Barth, T. J., and Frederickson, P. O. (1990). High-order solution of the Euler equations on unstructured grids using quadratic reconstruction, *AIAA*, Paper No. 90-0013.
4. Chen, Q., and Babuska, I. (1995). Approximate optimal points for polynomial interpolation of real functions in an interval and in a triangle. *Comp. Meth. Appl. Mech. Engrg.* **128**, 405–417.
5. Cockburn, B., and Shu, C. W. (1989). TVB Runge–Kutta local projection discontinuous Galerkin finite element method for conservation laws II: General framework. *Math. Comp.* **52**, 411–435.
6. Cockburn, B., Lin, S.-Y., and Shu, C. W. (1989). TVB Runge–Kutta local projection discontinuous Galerkin finite element method for conservation laws III: One-dimensional systems. *J. Comp. Phys.* **84**, 90–113.
7. Cockburn, B., Hou, S., and Shu, C. W. (1990). TVB Runge–Kutta local projection discontinuous Galerkin finite element method for conservation laws IV: The multidimensional case. *Math. Comp.* **54**, 545–581.
8. Colella, P., and Woodward, P. (1984). The piecewise parabolic method for gas-dynamical simulations. *J. Comp. Phys.* **54**.
9. Friedrich, O. (1998). Weighted essentially non-oscillatory schemes for the interpolation of mean values on unstructured grids. *J. Comp. Phys.* **144**, 194–212.
10. Godunov, S. K. (1959). A finite-difference method for the numerical computation of discontinuous solutions of the equations of fluid dynamics. *Mat. Sb.* **47**, 271.
11. Harten, A. (1983). High resolution schemes for hyperbolic conservation laws. *J. Comp. Phys.* **49**, 357–393.
12. Harten, A., Engquist, B., Osher, S., and Chakravarthy, S. (1987). Uniformly high order essentially non-oscillatory schemes III. *J. Comp. Phys.* **71**, 231.
13. Hu, C., and Shu, C. W. (1999). Weighted essentially non-oscillatory schemes on triangular meshes. *J. Comp. Phys.* **150**, 97–127.
14. Lax, P. D. (1954). Weak solutions of nonlinear hyperbolic equations and their numerical computation. *Comm. Pure Appl. Math.* **7**, 159–193.
15. Roe, P. L. (1981). Approximate Riemann solvers, parameter vectors, and difference schemes. *J. Comp. Phys.* **43**, 357–372.
16. Shu, C. W. (1988). Total-Variation-Diminishing time discretizations. *SIAM J. Sci. Statist. Comput.* **9**, 1073–1084.
17. Shu, C. W. (1987). TVB uniformly high-order schemes for conservation laws. *Math. Comp.* **49**, 105–121.
18. Shu, C. W., and Osher, S. (1989). Efficient implementation of essentially non-oscillatory shock-capturing schemes II. *J. Comp. Phys.* **83**, 32.
19. Wang, Z. J. (2002). Spectral (finite) volume method for conservation laws on unstructured grids: basic formulation. *J. Comp. Phys.* **178**, 210.
20. Wang, Z. J., and Liu, Y. (2002). Spectral (finite) volume method for conservation laws on unstructured grids II: Extension to two-dimensional scalar equation. *J. Comp. Phys.* **179**, 665–697.

Printed in Belgium